Journal of Power Sources 195 (2010) 5601–5605

Contents lists available at ScienceDirect

Journal of Power Sources

journal homepage: www.elsevier.com/locate/jpowsour

Short communication

Degradation behavior of anode-supported solid oxide fuel cell using LNF cathode as function of current load

Takeshi Komatsu*, Yoshiteru Yoshida, Kimitaka Watanabe, Reiichi Chiba, Hiroaki Taguchi, Himeko Orui, Hajime Arai

NTT Energy and Environment Systems Laboratories, Atsugi-shi, Kanagawa 243-0198, Japan

ARTICLE INFO

Article history:
Received 4 March 2010
Received in revised form 24 March 2010
Accepted 25 March 2010
Available online 31 March 2010

Keywords:
SOFC
Solid oxide fuel cell
Cathode
Degradation

ABSTRACT

We investigated the effect of current loading on the degradation behavior of an anode-supported solid oxide fuel cell (SOFC). The cell consisted of $LaNi_{0.6}Fe_{0.4}O_3$ (LNF), alumina-doped scandia stabilized zirconia (SASZ), and a Ni-SASZ cermet as the cathode, electrolyte, and anode, respectively. The test was carried out at 1073 K with constant loads of 0.3, 1.0, 1.5, and 2.3 A cm^{-2}. The degradation rate, defined by the voltage loss during a fixed period (about 1000 h), was faster at higher current densities. From an impedance analysis, the degradation depended mainly on increases in the cathodic resistance, while the anodic and ohmic resistances contributed very little. The cathode microstructures were observed using scanning electron microscopy (SEM) and transmission electron microscopy (TEM).

1. Introduction

Long-term stability is an important requirement for the practical use of solid oxide fuel cell (SOFC) systems, and the required lifetime is more than 40,000 h. Some groups have examined the durability of cells and stacks. Yokokawa et al. investigated the durability of different SOFC stacks/modules in the NEDO SOFC project [1–3]. Long-term (5000–10,000 h) tests were performed for stacks and modules to examine their durability. Horita et al. detected impurities at the cathode and the cathode–electrolyte interlayer using secondary ion mass spectrometry (SIMS) after a long-term operation test [4]. They found that the concentrations of several elements (Na, Al, Si, and Cr) increased with operation time. We also investigated the long-term stability of anode-supported cells with an LNF cathode that operated for over 6500 h [5]. We found that the degradation was caused by increases in the cathode polarization resistance and ohmic resistance. During a long-term test, elements (Si, B) from the sealant glass were detected in water condensed in the cathode exhaust gas.

Other groups undertook basic research to improve the durability and reliability of cells/stacks. Hatae et al. investigated the effect of current density on anode-supported cells during electrochemical oxidation [6]. The cells were operated under current densities of 0.025 and 0.25 A cm^{-2}. They found that the anode microstructure was changed by the electrochemical oxidation and redox cycles. Hagen et al. investigated the degradation behavior of anode-supported cells as a function of operating temperature and current density within 2000 h [7]. From an impedance analysis, they revealed that cathodic degradation was the dominant contribution to degradation at higher current densities (0.75 A cm^{-2}) and lower temperatures (1023 K). The anode was found to contribute more to degradation at higher temperatures (1133 K). According to Mosch et al., the degradation is mainly caused by the contact resistance between the anode and the cathode current collector during long-term operation (1000 h) and redox cycling [8]. Some research groups have reported Cr poisoning as a possible degradation source. The Cr oxide formed on the surface of the Cr-containing alloy separators during SOFC operation may migrate to and thus poison the cathode, resulting in the degradation of cell performance. Moreover, it was reported that the cell performance became worse at various current densities under Cr poisoning conditions [9]. These observations suggest that different cells, stacks, modules, and operating conditions induce various degradation factors in SOFC systems.

We have developed a planar anode-supported cell with a $LaNi(Fe)O_3$ (LNF) cathode. LNF is an attractive cathode material because of its high oxygen reduction activity at 1073 K, and also because it has a thermal expansion coefficient that matches that of zirconia electrolyte [10]. Furthermore, the reactivity of LNF to chromium species that can be generated from ferritic steel inter-

* Corresponding author at: NTT Corporation, NTT Energy and Environment Systems Laboratories, Morinosato-Wakamiya 3-1, Atsugi, Kanagawa 243-0198, Japan. Tel.: +81 46 240 2532; fax: +81 46 270 2702.
E-mail address: takeshi@aecl.ntt.co.jp (T. Komatsu).

0378-7753/$ – see front matter © 2010 Elsevier B.V. All rights reserved.
doi:10.1016/j.jpowsour.2010.03.078

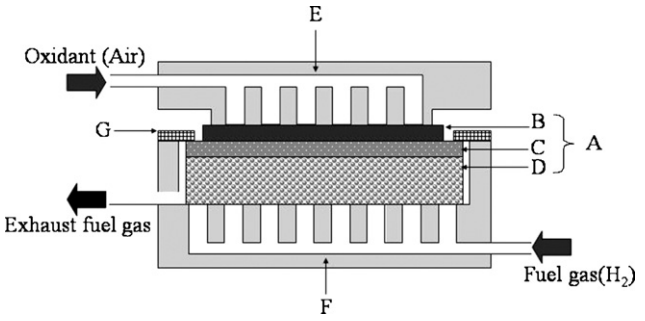

Fig. 1. Schematic illustration of testing equipment. (A) Cell; (B) cathode; (C) electrolyte; (D) anode; (E) metal alloy separator (cathode side); (F) metal alloy separator (anode side); (G) glass sealant.

connects is relatively low compared with other cathode materials [11]. A 50-cell stack with Φ 120-mm cells exhibits a 1 kW class electrical power output and a 54% conversion efficiency (gross DC, LHV) [12]. A single cell stack provides 60% (LHV) for more than 7000 h [13].

It was suggested that the degradation was caused by increases in the cathode polarization resistance and ohmic resistance. Therefore, we must investigate the lifetime and degradation factors in our cells. Moreover, it is also important to perform accelerated testing to establish the SOFC cell lifetime.

In this paper, we describe the electrochemical tests we performed on our anode-supported cell at 1073 K at different current densities to study the degradation factors under operating conditions.

2. Experimental

2.1. Cell fabrication

An anode-supported cell (Φ 60 mm) was fabricated by the co-firing method, which is described in detail elsewhere [14,15]. The electrolyte was 10 mol% Sc_2O_3- and 1 mol% Al_2O_3-stabilized ZrO_2 (SASZ). The anode was a mixture of 60 wt% NiO and 40 wt% SASZ. The anode and electrolyte green sheets were prepared by the doctor blade method. The electrolyte green sheet was laminated on the anode green sheet. The laminated sheet was then cut into disks, which were co-sintered at 1623 K to form half cells. The cathode was $LaNi_{0.6}Fe_{0.4}O_3$ (LNF). LNF paste was screen-printed on the electrolyte of the half cell and sintered. An LNF-GDC ($Ga_{0.2}Ce_{0.8}O_{1.9}$) interlayer was inserted between the electrolyte and cathode [16].

2.2. Electrochemical measurement

Electrochemical measurements were performed on the fabricated cell by using a metal alloy separator. Fig. 1 shows a cross-sectional image of the cell-separator testing equipment used for the anode-supported cell. The cell and anode separator were sealed together at the outer edge of the cell. Commercial borosilicate glass was used to join the ceramic cell and the separator. The tests were initiated by heating the cell in air to 1073 K at a heating rate of 50 K h^{-1}, and reducing the anode at this temperature in hydrogen (about 10%) and nitrogen, followed by pure hydrogen.

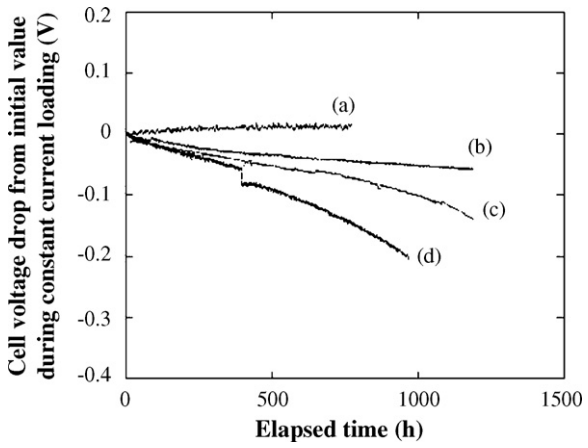

Fig. 2. Differences between cell voltages before and after loading constant current at densities of (a) 0.3 A cm^{-2}, (b) 1.0 A cm^{-2}, (c) 1.5 A cm^{-2}, and (d) 2.3 A cm^{-2}.

Accelerated degradation tests were carried out at 1073 K with constant loads of 0.3, 1.0, 1.5, and 2.3 A cm^{-2} (electrode area: 19.6 cm^2) as shown in Table 1. Pure hydrogen gas was used as the fuel on the anode. Dry air (P_{H_2O}: 1×10^{-7} atm) was used as the oxidant. The current–voltage curves and impedances were measured before and after the test under a constant current load, and the results are shown in Table 1. Impedance measurements were performed with a bias current of 1.8 A (0.09 A cm^{-2}) in a galvanostatic mode, with an AC amplitude of 200 mA. For this measurement, we used a frequency analyzer (Solatron 1260) and a potentiostat (Solatron SI1287).

2.3. Characterization

A microstructure analysis of the measured cells was conducted with scanning electron microscopy (SEM, JSM-890, JEOL), transmission electron microscopy (TEM, JEM-2100F, JEOL) and energy dispersive X-ray spectrometry (EDS, EX-23005BU, JEOL). For the TEM observation, thin specimens were vacuum embedded in epoxy resin and prepared using a focused ion beam (FIB) apparatus (SMI3050SE, SII NanoTechnology Inc.).

3. Results and discussion

3.1. Evaluation of electrochemical properties of cells under various loading conditions

The time dependences of the voltage for a cell when loading constant current densities of 0.3, 1.0, 1.5, and 2.3 A cm^{-2} and 1073 K are shown in Fig. 2. The voltage drop from its initial value was fairly linear with time at the lower current densities of 0.3 and 1.0 A cm^{-2}, and became more exponential at the higher current densities of 1.5 and 2.3 A cm^{-2} as shown in Fig. 2. For cell loading at 2.3 A cm^{-2}, a rapid cell voltage drop caused by thermal cycling was observed at about 400 h. However, in a series of tests, we found that the cell voltage drop with time depends on the current density.

Fig. 3 shows the *I–V* characteristics of the cell measured before and after the test under a constant current load of 2.3 A cm^{-2}. The

Table 1
Cell operating conditions.

No.	Constant current density (A cm^{-2})	O_2 utilization rate in air	H_2 utilization rate
1 reference data [4] (other experiment)	0.3	0.16	0.80
3	1.0	0.33	0.85
4	1.5	0.33	0.85
5	2.3	0.33	0.85

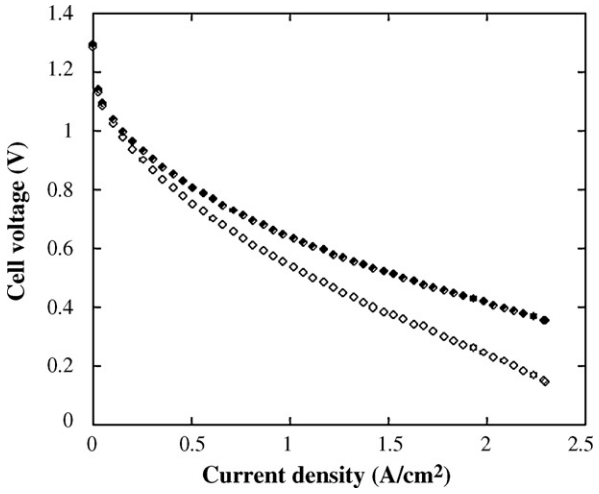

Fig. 3. *I–V* characteristics of the cell before (●) and after (○) loading constant current at density of 2.3 A cm^{-2}.

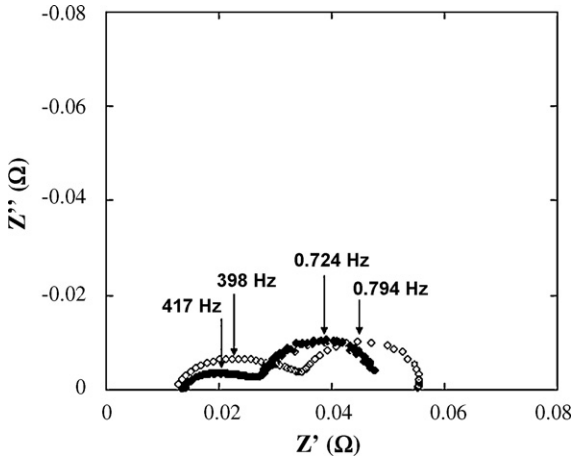

Fig. 4. Impedance spectrum for the cell before (●) and after (○) loading constant current at density of 2.3 A cm^{-2}.

I–V characteristics degraded in accordance with the voltage behavior during constant-current operation shown in Fig. 2. There was no sign of a drastic voltage reduction at 2.3 A cm^{-2} where the fuel utilization rate was 0.85. This suggests that anodic concentration overvoltage did not contribute dominantly to the cell performance in our series of measurements.

We measured the impedance spectrum to clarify the reason for the measured cell degradation. Fig. 4 shows impedance spectrums that we obtained before and after the measurements while loading a constant current density of 2.3 A cm^{-2}. There were two arcs on both spectrums. One arc was obtained at a high frequency (about 400 Hz) and the other was obtained at a low frequency (about 0.7 Hz). In our investigation, we found that the size of the high-frequency arc depends on the air conditions (ratio of oxygen pressure, gas flow rate), while that of the low-frequency arc depends on

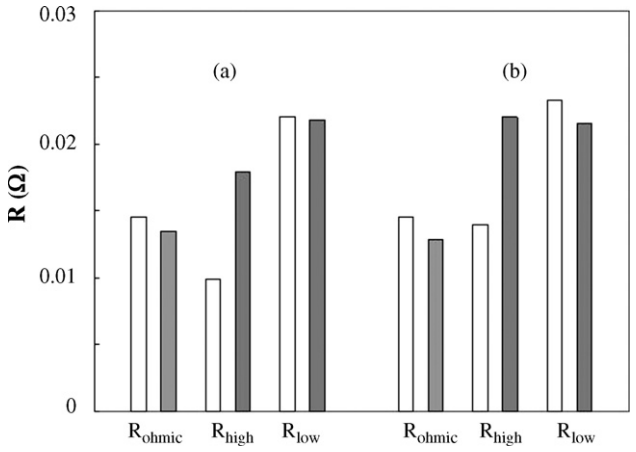

Fig. 5. Resistances for the cell estimated from impedance spectrum. (a) 1.5 A cm^{-2}, (b) 2.3 A cm^{-2}. R_{ohmic}: ohmic resistance, R_{high}: cathode resistance, R_{low}: anode resistance, (□): before constant current loading, (■): after constant current loading.

the fuel gas condition. Therefore, we assigned the resistances for the cathode and anode polarizations to the high- and low-frequency arcs, respectively. We also estimated the ohmic resistance. The size for a high-frequency arc was larger after loading a constant current. On the other hand, the size for a low-frequency arc remained almost unchanged. Fig. 5(a) and (b) shows the resistances of the cell obtained from the impedance spectrum before and after the test for current densities of 1.5 and 2.3 A cm^{-2}, respectively. The cathode resistance (R_{high}) increased considerably after loading the current, while the anodic resistance (R_{low}) and ohmic resistance (R_0) decreased slightly. This showed that the degradation of the *I–V* characteristics was caused by increasing the cathodic resistance. Moreover, it suggested that the cell on the anode side was relatively stable because the anodic resistance was almost constant under high current density and high fuel utilization conditions.

3.2. Observation of cathode microstructure with SEM and TEM

We observed the cathode microstructure after the constant current loading measurements to examine the increase in cathode resistance. Fig. 6 shows SEM images of the cathode microstructure before and after the measurements. The shapes of the particles composing the cathode microstructure (Fig. 6(b) and (c)) had clearly changed after the measurement (Fig. 6(a)). We found that the particles coalesced with each other. This indicates that the cathode particles were coalesced by the constant current loading. Hence, the coalescing of the cathode particles appears to play a dominant role in reducing the active sites of the triple phase boundary (TPB) and increasing the resistance.

Moreover, an unknown layer was observed at the interface between the cathode and the electrolyte for the cell operated at 2.3 A cm^{-2} as shown in Fig. 6(c). No layer was observed in other measurements. A cross-sectional TEM/EDX analysis was conducted to analyze the unknown layer. Fig. 7 shows a TEM image of the cathode/electrolyte interface for a cell operated at 2.3 A cm^{-2} after the electrochemical measurements. Results of EDX analyses at the indi-

Table 2
EDX spectrum of the measured cell operating at 2.3 A cm^{-2}.

EDX point	O	Al	Sc	Cr	Fe	Ni	Zr	La	Ce	Gd	SUM (at.%)
1	18.3	0.28	0.99	2.55	9.09	3.82	2.04	46.57	15.13	1.25	100
2	21.51	0.05	0.21	25	0.52	0.63	7.49	2.81	39.38	2.41	100
3	20.35	0.15	0.34	14.16	0.16	0.14	2.74	7.45	50.74	3.76	100
4	17.58	0.11	0.41	23.71	0.06	0.34	5.99	4.68	44.02	3.11	100
5	8.73	0.09	6.52	0.11	0.05	0.24	83.94	0.07	0.12	0.14	100

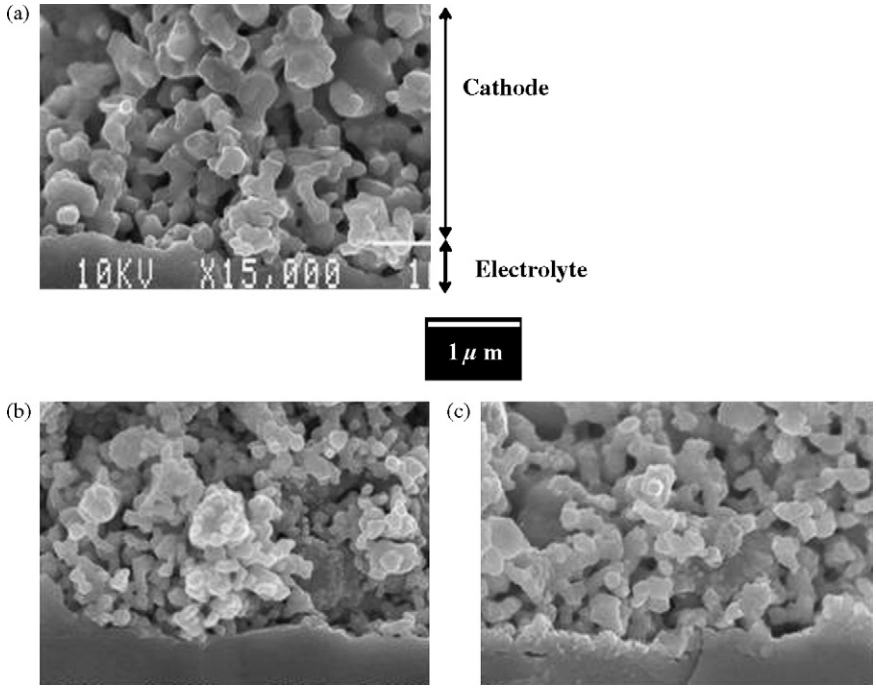

Fig. 6. Cross-sectional SEM images of measured cell. (a) Before measurement, (b) after measurement operating at 1.5 A cm^{-2}, and (c) after measurement operating at 2.3 A cm^{-2}.

cated locations are given in Table 2. According to the TEM and EDX analyses, the unknown layer was about 0.3 μm thick and Cr was detected strongly at the EDX point (2–4). This suggested that the unknown layer was a Cr related species.

We consider that the Cr species evaporated from the alloy separators. This phenomenon is called Cr poisoning [17]. The Cr species was deposited at active sites at the interface, and this caused the degradation of the electrochemical performance. Moreover, it has been reported that the cell degradation accelerated at a higher current density under Cr poisoning conditions [9]. They reported that it takes about 50 and 350 h for a voltage drop of 200 mV for a cell with an LSM cathode at constant current densities of 0.12 and 0.345 A cm^{-2}, respectively. We therefore attribute the exponential degradation behavior observed with the sample under 2.3 A cm^{-2} loading to Cr poisoning. However, with our measurement at 2.3 A cm^{-2}, it took 1000 h for a cell voltage drop of 200 mV. This suggests that the LNF cathode was relatively stable against Cr poisoning.

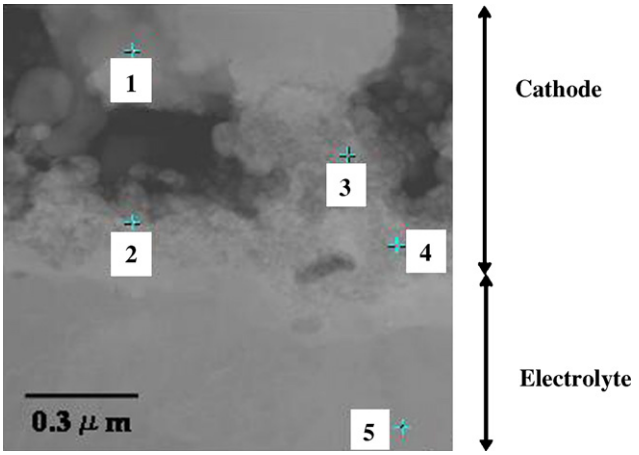

Fig. 7. TEM image of measured cell operating at 2.3 A cm^{-2}.

A series of the above measurements suggested two possible degradation factors (the condensation of cathode particles and Cr poisoning) after the cell were operated at a high current density. Moreover, if these two degradation factors appear in the long-term test at a low current density, an examination of loading with a high current density offers the potential for use as an accelerated test for estimating cell lifetime.

4. Conclusion

We carried out electrochemical tests on anode-supported SOFCs at 1073 K at different current densities. The cell voltage decreased linearly at current densities of 0.3, 1.0 and 1.5 A cm^{-2}, and exhibited exponential behavior at 2.3 A cm^{-2}. An analysis of the impedance spectrum showed that the cathodic resistance increased. The ohmic and anode resistances were not greatly changed. We found that the electrochemical performance on the cathode side was affected by degradation processes. SEM and TEM/EDX observations revealed that the cathode particles coalesced owing to the constant current loading, and a Cr species layer was observed in the vicinity of the cathode/electrolyte interface in a measurement at a high current density of 2.3 A cm^{-2}.

References

[1] H. Yokokawa, T. Horita, N. Sakai, K. Yamaji, M.E. Brito, Y.P. Xiong, H. Kishimoto, Solid State Ionics 177 (2006) 3193–3198.
[2] H. Yokokawa, T. Watanabe, A. Ueno, K. Hoshino, ECS Trans. 7 (1) (2007) 133–140.
[3] H. Yokokawa, T. Horita, K. Yamaji, H. Kishimoto, Y.P. Xiong, M.E. Brito, Proceedings of 8th European SOFC Forum, 2008, p. B1004.
[4] T. Horita, H. Kishimoto, K. Yamaji, M.E. Brito, Y. Xiong, H. Yokokawa, Y. Hori, I. Miyachi, J. Power Sources 193 (2009) 194–198.
[5] T. Komatsu, K. Watanabe, M. Arakawa, H. Arai, J. Power Sources 193 (2009) 585–588.
[6] T. Hatae, Y. Matsuzaki, S. Yamashita, Y. Yamazaki, Solid State Ionics 180 (2009) 1305–1310.
[7] A. Hagen, R. Barfod, P.V. Hendriksen, Y. Liu, S. Ramousse, J. Electrochem. Soc. 153 (2006) A1165–A1171.
[8] S. Mosch, N. Trofimenko, M. Kusnezoff, T. Betz, M. Kellner, ESC Trans. 7 (1) (2007) 381–388.

[9] S. Taniguchi, M. Kadokawa, T. Yasuo, Y. Akiyama, Y. Itoh, Y. Miyake, K. Nishio, Denki Kagaku 64 (1996) 568.
[10] R. Chiba, F. Yoshimura, Y. Sakurai, Solid State Ionics 124 (1999) 281–288.
[11] T. Komatsu, R. Chiba, H. Arai, K. Sato, J. Power Sources 176 (2008) 132–137.
[12] M. Yokoo, Y. Tabata, Y. Yoshida, H. Orui, K. Hayashi, Y. Nozaki, K. Nozawa, H. Arai, J. Power Sources 184 (2008) 84–89.
[13] Y. Yoshida, T. Komatsu, R. Chiba, M. Yokoo, K. Hayashi, H. Orui, H. Arai, ECS Trans. 25 (2) (2009) 421–428.
[14] H. Orui, K. Watanabe, R. Chiba, M. Arakawa, J. Electrochem. Soc. 151 (2004) A1412–A1417.
[15] H. Orui, K. Nozawa, K. Watanabe, S. Sugita, R. Chiba, T. Komatsu, H. Arai, M. Arakawa, J. Electrochem. Soc. 155 (2008) B1100–B1116.
[16] R. Chiba, H. Orui, T. Komatsu, Y. Tabata, K. Nozawa, M. Arakawa, K. Sato, H. Arai, J. Electrochem. Soc. 155 (2008) B575–B580.
[17] S.P. Jiang, J.P. Zhang, L. Apateanu, K. Foger, J. Electrochem. Soc. 147 (2000) 4013–4022.